Cellular and Molecular Biology
E-ISSN : 1165-158X / P-ISSN : 0145-5680
www.cellmolbiol.org

Molecular Subtypes Based on PANoptosis Genes and Characteristics of Immune Infiltration in Cutaneous Melanoma

Like Zhong, Wenkang Qian, Wangang Gong, Li Zhu, Xu Wang*

Zhejiang Cancer Hospital, Hangzhou Institute of Medicine (HIM), Chinese Academy of Sciences, Hangzhou, Zhejiang 310022, China

ARTICLE INFO

Original paper

Article history:
Received: August 06, 2022
Accepted: June 07, 2023
Published: August 31, 2023

Keywords:

Cutaneous melanoma, PANoptosis, molecular subtypes, prognosis, immune infiltration

ABSTRACT

Cutaneous melanoma (CM) remains the most life-threatening form of skin cancer. Further risk stratification and search for new prognostic targets for CM are of positive clinical significance. PANoptosis is defined as an inflammatory programmed cell death mediated by the PANoptosome complex and cannot be characterized by pyroptosis, apoptosis or necroptosis alone. Although PANoptosis is closely associated with many diseases including cancer, it has not been reported in CM. Combined with GTEx and TCGA database, we extracted 14 PANoptosis-related genes (PAGs). The molecular subtypes of CM were then analyzed by PAGs and their associations with the immune microenvironment and immunotherapy reactivity were analyzed. LASSO and univariate Cox analysis was performed on PAGs-related differentially expressed genes to establish PAGs characteristics that could effectively predict the prognosis of CM patients. Immune infiltration, tumor mutation burden analysis, immunotherapy response and drug sensitivity analysis were used to further analyze the causes of prognostic differences. Our study provides a new perspective on the role of PANoptosis in CM.

Doi: http://dx.doi.org/10.14715/cmb/2023.69.8.1

Introduction

Cutaneous melanoma (CM) remains the most life-threatening form of skin cancer, with an annual increase of more than 3% (1). Melanin pigmentation and melanogenesis are important phenotypic characteristics of melanoma (2, 3). Recent advances in immune checkpoint inhibitors (ICIs) and targeted therapies have led to significant improvements in long-term survival in CM patients (4). However, although the scientific advances in CM therapy have been significant, approximately two-thirds of patients treated with immune checkpoint monotherapy progressed (5). During the carcinogenesis process, melanoma develops multiple mechanisms to overcome chemotherapy and immunotherapy. In addition to affecting melanin pigmentation and melanogenesis (6, 7), multiple methods can also affect the therapeutic effect, including neuro-regulatory factors and corticosteroids producing (8), drug sensitivity regulation (9), cell metabolism regulation (3). In view of the incomplete clinical efficacy, it is of positive clinical significance to further evaluate the possible prognostic-related mechanisms and their impacts on clinical efficacy.

Following the discovery and demonstrated biological functions of multiple programmed cell death (PCD) types, increasing evidences have shown extensive interactions between these programmed cell deaths, including pyroptosis, apoptosis and necroptosis (10-13). PANoptosis was defined in 2019 as an inflammatory PCD pathway mediated by the PANoptosome complex with key features of pyroptosis, apoptosis and/or necroptosis that cannot be explained by a single PCD. PANoptosome is a multi-protein complex that acts as a scaffold platform for the activation of key molecules in the pyroptosis, apoptosis and necroptosis processes (14). The study of PANoptosis is still in its infancy and several important targets have been identified to mediate its activation, including AIM2, CASP family, ZBP1, RIPK1/3 and IRF1 (15).

PANoptosis is now known to be closely linked to a number of diseases, including cancer. PANoptosis has been shown to have the potential to kill cancer cells (16). Although there is no direct evidence of the role of PANoptosis in CM, several key factors of the PANoptosis process are associated with tumor progression. Caspase-6 plays a crucial role in human tumorigenesis by regulating PANoptosis and may be an important target for tumor prevention and treatment (17). Z-DNA binding protein 1 (ZBP1) is a key factor in PANoptosis that initiates the assembly of PANoptosome (10, 18), which is positively associated with tumor aggressiveness in breast cancer. In addition, interferon regulatory factor 1 (IRF1) is recently identified as a key regulatory factor in the tumor-associated PANoptosis pathway (19). As an essential transcription factor for the programmed cell death ligand 1 (PD-L1) gene, IRF1 plays a central role in innate and adaptive immunity and is also involved in tumor progression (20). Therefore, the above evidence suggests that it is necessary to (20) further clarify the role of PANoptosis in CM.

In today's era of "big data" and personalized medicine, bioinformatics has been shown to help increase our understanding of CM heterogeneous nature (21). In this study, we analyzed the molecular subtypes of CM based on PANoptosis-associated genes (PAGs) and further analyzed the correlation between different molecular subtypes and immune microenvironments and immunotherapy reactivity. After screening for PAGs with differentially expressed molecules, a PAGs signature was established that could

* Corresponding author. Email: wxkingsun@sina.com

effectively predict prognosis in CM patients. Immunoinfiltration analysis, tumor mutation burden (TMB), immunotherapy and drug sensitivity analysis were used to further analyze the reasons for the difference in signature prognosis. Our study provides a new perspective on the role of PANoptosis in CM.

Materials and Methods

Data Acquisition

The publicly accessible transcriptome data of CM was acquired from the GTEx, TCGA and GEO databases. The expression data of skin normal tissues was extracted from the UCSC Xena database (https://xenabrowser.net/datapages/). Transcriptome data of CM was acquired from the TCGA and GEO database, with 471 samples (1 normal sample and 470 CM samples) in TCGA-SKCM and 214 CM samples in GSE65904. The clinical information corresponding to each sample was obtained from the TCGA and GEO databases, excluding those without survival time, and we included 668 samples for the study in total. The R package "sva" was performed to remove the batch effect of the transcriptome data and merged the files into the final matrix. The copy number variation (CNV) and tumor mutation burden (TMB) files (maf format) of CM were got from the TCGA database.

Difference analysis and protein-protein interaction (PPI) network analysis

A total of 14 PANoptosis-associated genes (PAGs) were obtained from the previous literature (22). The difference expression analysis of the PAGs in normal and tumor tissues was performed at $|\text{fold change}| \geq 1$, and $P < 0.05$. The STRING database was utilized to explore the protein-protein interaction of PAGs (https://cn.string-db.org/). RCircos package was conducted the display the location of PAGs in the chromosome in the R landscape environment. The CNV of PAGs was extracted from the TCGA dataset, including two types of PAGs (amplification and deletion). Maftools package was adopted to exhibit the mutation frequency of PAGs for CM.

Unsupervised consensus clustering analysis for PAGs subgroups

An unsupervised consensus clustering analysis was developed to explore the molecular pattern for CM. According to the expression profile of PAGs in CM, the ConsensusClusterPlus package was used to cluster the CM samples into different molecular subgroups. The association of PAGs expression profile, clinical characteristics, and clinical prognosis outcome was generated via the "pheatmap" package. "survival" package was adopted to explain the overall survival (OS) rate of CM in the different molecular patterns. Principal component analysis (PCA) was carried out to explore the distribution pattern of PAGs-based molecular pattern via the "ggplot2" package. The gene set variation analysis (GSVA) was practiced to explore the KEGG terms of the molecular pattern referenced to the gene set (c2.cp.kegg.v7.4.gmt).

Characteristic of the tumor microenvironment (TME)

ESTIMATE algorithm was used for evaluating the immune cell and stromal score of CM. Second, by calculating the gene matrix and the proportion of 23 immune cell marker genes, we obtained the percentage of 23 immune cells for CM via ssGSEA algorithm. A Limma package was conducted to visualize the immune checkpoints (ICPs) expression.

Generation of the differential expression genes in molecular subtypes pattern

To explore the differential expression genes (DEGs) in the PAGs-based molecular pattern, we conducted "limma" package to calculate the DEGs between the molecular pattern with the threshold set at $|\text{fold change}| > 2$ and $P < 0.05$. Then, the intersection genes between different molecular subgroups were screened via the "VENN" package. clusterProfiler package was adopted to investigate the molecular function and enriched the DEGs into gene ontology (GO) and Kyoto Encyclopedia of Genes and Genomes (KEGG).

Development and validation of the PAG score

In first, the PAGs-based subgroups DEGs were enrolled to develop the PAG score of each CM sample. On the basis of "LASSO" and univariate Cox analysis (uniCox) algorithm, the characteristic variates associated with OS rate were obtained. Second, those important variates were enrolled for multivariate Cox analysis to explore the independent prognostic variates. The PAG score of CM was explored as the following calculation formula: PAG score = CST7 x -0.823 + NAGK x 2.389 + FBXO6 x -0.835 + PSME1 x -2.093 + USP3 x -1.138 + RTN1 x -0.581. According to the median value division, the PAG score of CM was classified in low- and high-PAG score groups. To validate the independence and accuracy of the PAG score for CM, a caret package was carried out to divide the CM samples into training cohort and test cohort with the criteria set at 7:3. Then, the PAG score of the training cohort and test cohort was calculated according to the important variates, respectively. pheatmap package was applied to display the association of PAG score and clinical prognosis outcome for CM.

Nomogram construction and clinicopathological subgroups analysis

Integration of clinical information from TCGA-SKCM and GSE65904, we developed a nomogram model to evaluate the 1-, 3-, and 5-year clinical survival probability of CM via "rms" package. Univariate/multivariate Cox analysis was carried out to explore the independence of PAG score and clinical features (age and gender). The TimeROC package was used to investigate the time-dependent ROC curve at 1-, 3-, and 5-year. Regplot package was performed to explore the calibration curve of the clinical survival outcome predicted by nomogram and actual clinical survival outcome. The Concordance index (C-index) was carried out to evaluate the accuracy of the PAG score and clinical features in predicting clinical survival outcomes for CM via "rms" and "pec" packages. On the basis of the PAG score, the clinical survival outcomes of CM in age and gender with low- and high-PAG scores were explored via the "survival" package.

Immunotherapy response, tumor mutation burden and chemotherapy drug prediction

Based on expression profiles of CM, the tumor immune dysfunction and exclusion (TIDE) was predicted to eva-

luate the immunotherapy response for CM (http://tide.dfci.harvard.edu/). The cancer immunome atlas (TCIA) database was used to explore the immunotherapy response for PD-1 and CTLA-4 (https://tcia.at/home). Tumor mutation burden (TMB) files of CM were downloaded from the TCGA database, and the TMB matrix of low- and high-PAG score groups was extracted in the Perl language environment. Maftools package was carried out to explore the top 15 somatic mutation frequencies in low- and high PAG score groups. The chemotherapy drug sensitivity of CM was predicted by genomics of drug sensitivity in cancer (GDSC) database via pRRophetic package.

Statistical analysis

All data analysis for this study was carried out in R language environment (https://cran.r-project.org/). The statistical analysis between two groups was performed using Wilcoxon rank-sum test analysis, or ANOVA statistical analysis if there were more than two groups. Spearman's correlation was used to count the correlation between the PAG score and immune cells. $P < 0.05$ was considered statistically different.

Results

Analysis of PAGs expression and mutation frequency in CM

Combined with GTEx and TCGA database, we extracted 14 PAGs to explore the role of PAGs in CM tumourigenesis and development. The difference analysis of PAGs suggested that the expression of ZBP1, NLRP3, RIPK1, CASP6 and FADD were overexpressed in tumor tissues, whereas the expression of RIPK3, CASP8, PYCARD, MAP3K7, TNFAIP3, RNF31, and PSTPIP2 were higher in normal tissues (Figure 1A). PPI network analysis showed a clear association between 14 PAGs (Figure 1B). Somatic mutation analysis revealed the mutation landscape of PAGs, and the result showed that the frequency of NLRP3 was 10%, which was the highest mutation gene in CM (Figure 1C). In addition, the circle diagram showed the position of PAGs on the chromosome (Figure 1D). As shown in Figure 1E, the CNV frequency of 14 PAGs suggested that 4 PAGs (FADD, RIPK1, NLRP3 and ZBP1) demonstrated CNV amplifications, whereas 4 PAGs (CASP1, TNFAIP3, CASP6 and MAP3K7) showed CNV deletions. According to univariate Cox analysis, the correlation of PAGs expression and prognostic significance was illustrated in a network (Figure 1F). A clear correlation among 14 PAGs expression levels was observed; a negative correlation was explored between PYCARD and MAP3K7, and a positive correlation was observed in other PAGs. Moreover, the Cox test result identified 8 PAGs as favorable factors for CM ($P < 0.05$). These findings demonstrated the potential role of PAGs in the development of CM and were associated with mutation burden, prognosis and CNV.

PAGs-based subgroup analysis and TME evaluation of CM

668 CM samples were enrolled from the TCGA and GEO databases to investigate the relationship of PAGs and tumourigenesis. To determine the potential association between PAGs and CM subgroups, we conducted a consensus clustering analysis to classify the CM patients based on the expression profiles of PAGs. Under the condition of unsupervised classification, the CM patients were clustered into 3 subgroups, including 206 samples in cluster A, 185 samples in cluster B, and 277 samples in cluster C (Figure 2A). In 3 unsupervised classifications, a significant difference of clinical outcome was observed for CM. The Kaplan-Meier survival curve suggested the OS rate in cluster C was better than those in cluster B and C ($P = 0.002$, Figure 2B). PCA result also demonstrated significant separation between the 3 subgroups, indicating the

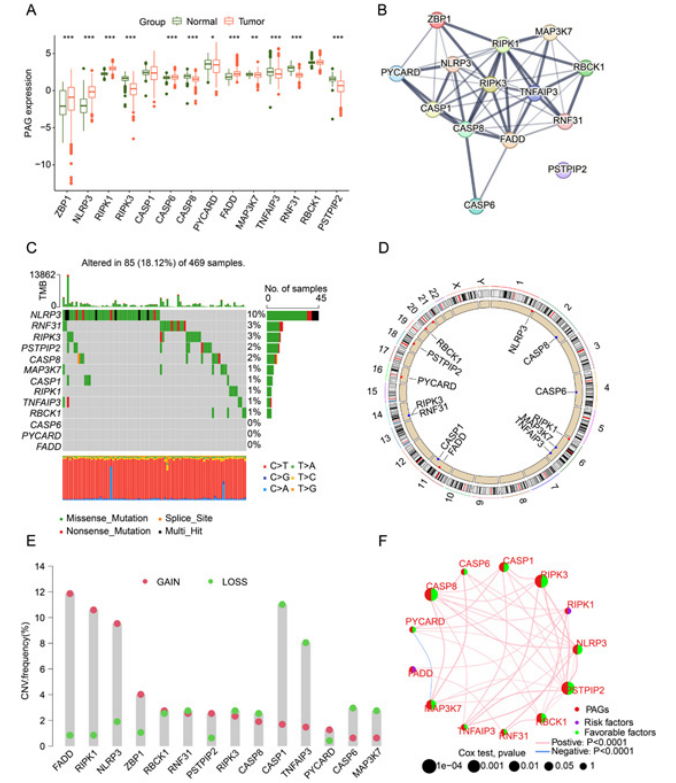

Figure 1. Analysis of PAGs expression and somatic mutation landscape in CM. (A) The expression of PAGs in normal tissues and tumor tissues for CM. (B) PPI network analysis of PAGs. (C) Mutation frequency of PAGs in CM. (D) The circle diagram shows the location of PAGs on the chromosome. (E) CNV frequency of PAGs (gain, loss). (F) Correlation analysis of PAGs and prognostic for CM.

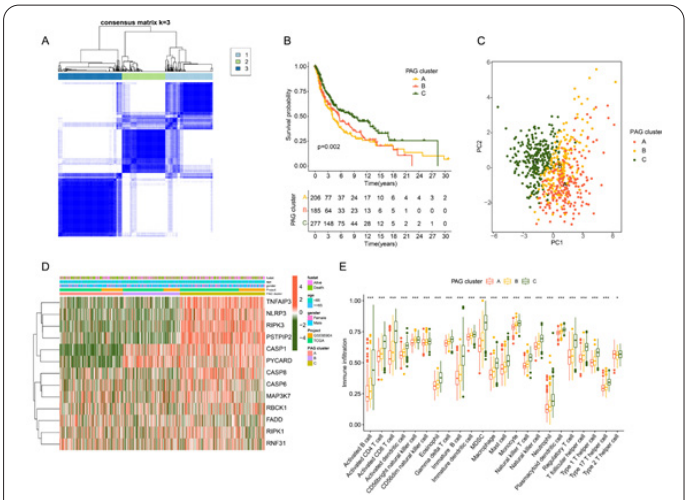

Figure 2. PAGs subgroups identification and TME landscape of CM. (A) Consensus clustering analysis of CM patients. The consensus matrix = 3. (B) Kaplan-Meier analysis of CM samples in cluster A, B, and C. (C) PCA plot of 3 PAGs-based subgroups. (D) Expression of PAGs and clinical features of CM in 3 PAGs-based subgroups. (E) Immune infiltration score of 23 immune cells in cluster A, B, and C.

unsupervised classification of CM was accurate (Figure 2C). The expression of 14 PAGs and clinical features of CM patients in 3 subgroups were further explored, and the result indicated a substantial difference of PAGs expression and clinical features in different PAGs subgroups (Figure 2D). We further estimated the relationship between TME and PAGs. The ssGSEA result suggested that the immune infiltration score of 23 immune cells was greatly higher in cluster C than in cluster A and B, showing an immune activation status of CM patients in cluster C (Figure 2E). These results revealed that the CM patient could be classified into 3 independent subgroups based on PAGs, and correlated with prognosis and immune infiltration.

Characteristic of immunotherapy response in different PAGs-based subgroups

Considering the potential association between PAGs and the immune-infiltration landscape, the immunotherapy responses of CM in 3 subgroups were further estimated. According to GSVA analysis, a remarkable difference in immune-related signaling pathways was observed in 3 PAGs-based subgroups, such as the T cell receptor signaling pathway, the T cell B receptor signaling pathway, and the Toll like receptor signaling pathway (Figure 3A, B). The ESTIMATE score suggested that the stromal, immune, and ESTIMATE scores of CM in cluster C were significantly higher than cluster A, and cluster B, whereas tumor purity was lower in cluster C, showing a better immune and stromal status for CM in cluster C (Figure 3C-F). TIDE result revealed that the CM patients in cluster C had the highest TIDE score than cluster A and B, indicating a worse response for immunotherapy for CM in cluster C (Figure 3G). Additionally, we evaluated the response to CTLA-4 and PD-1 treatment of CM in 3 subgroups, and the results illustrated that the CM patients in cluster C were more sensitive to CTLA-4, PD-1, and CTLA-4/PD-1 treatment (Figure 3H-J).

Generation of gene subgroups based on PAGs associated DEGs

In order to further explore the potential molecular function of PAGs subgroups in CM, we developed a difference analysis to identify DEGs in 3 PAGs-based subgroups via "limma" R package. With the threshold set at $P < 0.001$, 148 PAGs-associated DEGs were identified among the 3 subgroups. KEGG enrichment analysis suggested that the DEGs were greatly enriched in antigen processing and presentation, epstein−Barr virus infection, and phagosome (Figure 4A). GO analysis indicated that lymphocyte-mediated immunity, antigen processing and presentation, and MHC protein complex were enriched, which is associated with immune response (Figure 4B). Consensus clustering was carried out to cluster the CM samples based on the DEGs, and 2 unsupervised classifications were calculated, with 331 samples in gene-cluster A and 337 samples in gene-cluster B. As shown in Figure 4C, the CM patients in gene-cluster A had better clinical outcomes than those in gene-cluster B ($P < 0.001$, Figure 4C). The PCA plot suggested a clear distinction within the group among gene-cluster A and B (Figure 4D). In addition, the expression level of DEGs and clinical features illustrated remarkable differences between the 2 gene-cluster subgroups (Figure 4E). The result of PAGs in the 2 gene-cluster subgroups showed that the expression level of NLRP3, RIPK3, CASP1, CASP6, CASP8, PYCARD, TNFAIP3, RBCK1, and PSTPIP2 was higher in the gene-cluster B; however, the expression level of FADD was higher in gene-cluster A (Figure 4F).

Construction of the PAGs signature

To further investigate the characteristic of PAGs in the development of CM, we conducted a LASSO model to identify the feature PAGs associated with DEGs to construct the PAGs signature for CM. According to the univariate Cox analysis, 110 PAGs associated DEGs were identified as prognostic factors for CM; moreover, LASSO analysis was utilized to determine the optimal lambda value of prognostic factors, 9 feature variates were obtained. The PAG score was established based on the expression level and coefficient of 6 prognostic factors which were calculated by multivariate Cox analysis. According to the 6 prognostic factors, the CM samples were classified into training cohort (468 CM samples) and test cohort (200 CM samples) with the cutoff set at 7:3. In the PAGs cluster, a lower PAG score was observed in cluster C than cluster

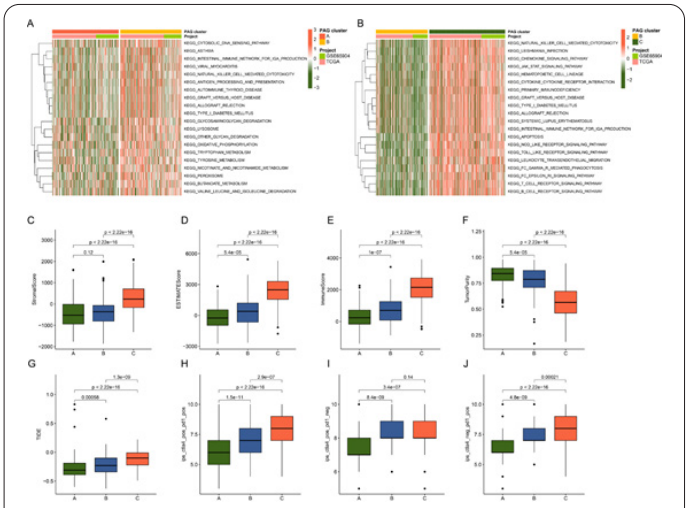

Figure 3. Characteristic of immunotherapy response in PAGs-based subgroups. (A, B) GSVA algorithm shows the KEGG signaling pathways. (C-F) ESTIMATE score in 3 PAGs-based subgroups. (G) TIDE score. (H-J) IPS score shows the response to CTLA-4 and PD-1 for CM.

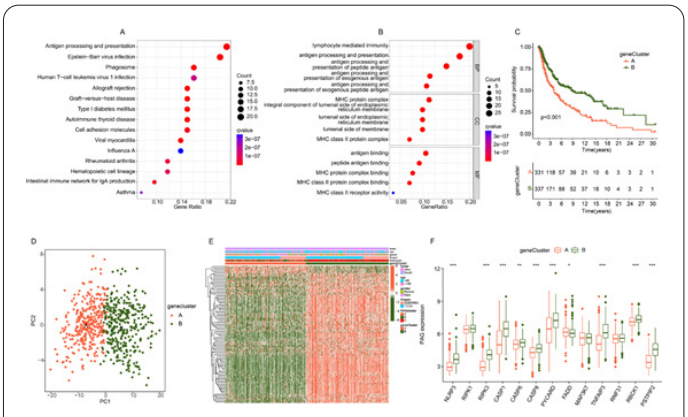

Figure 4. Characteristic of gene subgroups based on PAGs associated with DEGs. (A) KEGG and (B) GO enrichment analysis of PAGs associated DEGs. (C) The Kaplan-Meier analysis of 2 unsupervised clustering. (D) PCA plot of 2 unsupervised gene-cluster for CM. (E) Characteristics of DEGs and clinical features in PAGs cluster and gene-cluster subgroups. (F) The expression level of PAGs in gene-cluster A and B.

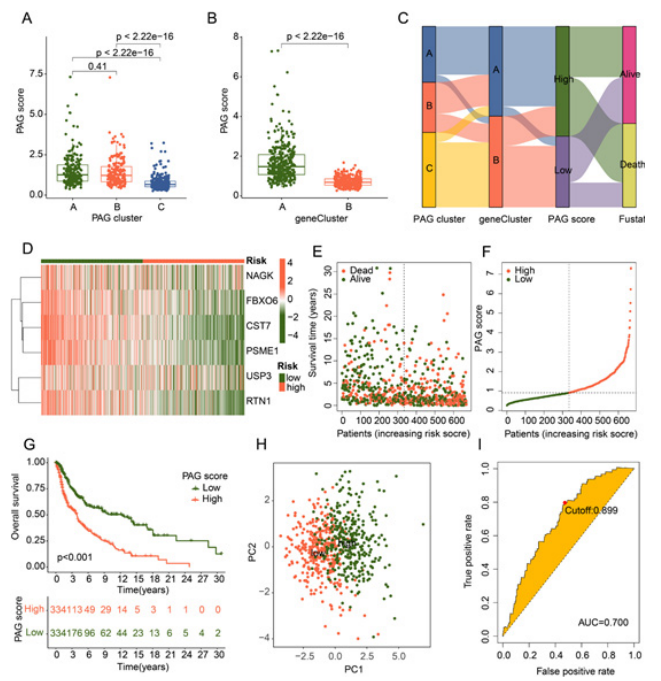

Figure 5. Construction of PAG signature of CM. (A) Distribution of PAG score in PAG clustering subgroups. (B) Difference analysis of PAG signature in gene-cluster subgroups. (C) The alluvial diagram shows the relationship between the PAG cluster, gene cluster, PAG score and survival status. (D) The expression level of 6 prognostic signature in low PAG score and high PAG score groups. (E, F) Classification of CM samples with low PAG and high PAG scores. (G) Survival curve of CM samples in two PAG score groups. (H) PCA plot shows two different classifications between the low PAG score and high PAG score groups. (I) ROC curve of PAG score for CM. The cutoff is 0.899.

A and B (Figure 5A). As for gene cluster subgroups, the PAG score was also lower in cluster B than in cluster A (Figure 5B). These results suggested that the high PAG score was positively related to poor prognosis. The alluvial plot showed the relationship of CM between the PAG cluster, gene cluster, PAG score and survival status (Figure 5C). As displayed in Figure 5D, the expression level of 6 prognostic factors was markable higher in the low PAG score group than those in the high PAG score group. In the entire risk cohort, the CM samples were divided according to the median PAG score (Figure 5E, F). The Kaplan-Meier analysis suggested that the CM patients in the low PAG score group had better survival outcomes than the high PAG score (Figure 5G). In the training cohort and test cohort, we observed the same survival outcome of CM patients in the low PAG score group and high PAG score group. PCA diagram revealed that the PAG score could accurately classify the CM samples (Figure 5H). Moreover, the AUC of the PAG score was 0.700, showing a good diagnostic ability for CM (Figure 5I).

Development of nomogram to predict prognosis for CM

The relationship between PAG score and clinical characteristics was determined via univariate/multivariate Cox analysis, and the results suggested that the PAG score was an independent factor for CM (univariate: HR = 1.547 (1.398-1.713), P < 0.001; multivariate: HR = 1.549 (1.399-1.714), P < 0.001, Figure 6A, B). The curve of the concordance index (C-index) showed that the C-index of the PAG score was greatly higher than age and gender, indicating a good predictability in estimating prognosis for CM (Figure 6C). According to the clinical features and PAG score, we established a nomogram to assess the survival probability of CM at 1-, 2-, and 3 years (Figure 6D). The time-dependent ROC curve showed that the AUC of 1-, 2-, and 3 years was 0.700, 0.697, and 0.667, respectively (Figure 6E). Moreover, the calibration curve revealed a high consistency between the nomogram-predicted OS rate and the actual OS (Figure 6F). In the different clinical features, the survival outcome of CM with low PAG score and high PAG score was further evaluated and the result demonstrated that the CM in the low PAG score group had a better OS rate than those in the high score group among the age and gender (Figure 6G-J).

The Characteristics of TME and TMB in PAG score subgroups

The relationship between PAG score and TME characteristics was further explored. According to the GSVA analysis, a series of immune-related signaling pathways were markedly downregulated in the high PAG score group, involving primary immunodeficiency, chemokine signaling pathway, natural killer cell-mediated cytotoxicity, and toll-like receptor signaling pathway (Figure 7A). Immune and stromal status analysis revealed that the CM patients in the low PAG score group had higher ESTIMATE, stromal, and immune scores, and lower tumor purity than those in the high PAG score group (Figure 7B-E). Immune infiltration assessment results suggested that the low PAG score group had higher immune status than the high PAG score group, such as activated B cell, CD4 + T cell, CD8 + T cell, NK T cell, NK cell, and eosinophil (Figure 7F). Additionally, correlation analysis between the PAG score and immune infiltration suggested that the PAG score was negatively related to the immune status (Figure 7G).

The characteristic of TMB in low- and high PAG score

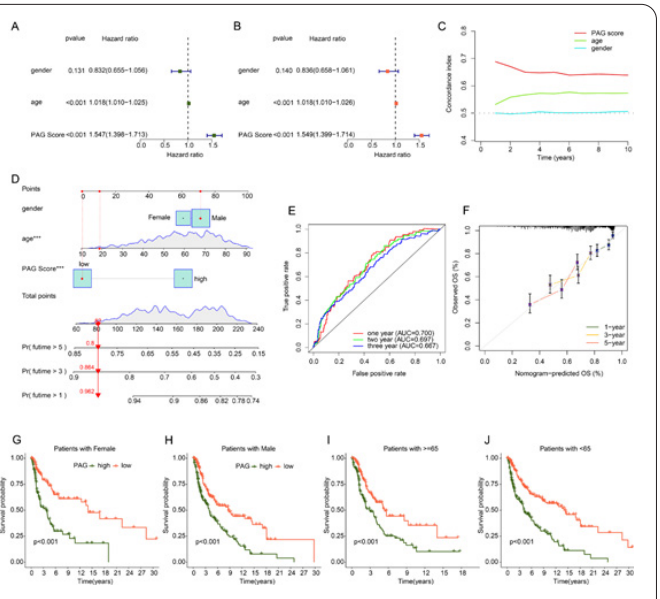

Figure 6. Development of nomogram and independence analysis. (A, B) Independence analysis of PAG score. (C) Concordance index of PAG score, age, and gender. (D) Nomogram development of PAG score and clinical features. (E) Time-dependent ROC curve at 1-, 2-, and 3 years. (F) Calibration curve. (G-J) Survival curve of CM samples with low PAG score and high PAG score among age and gender.

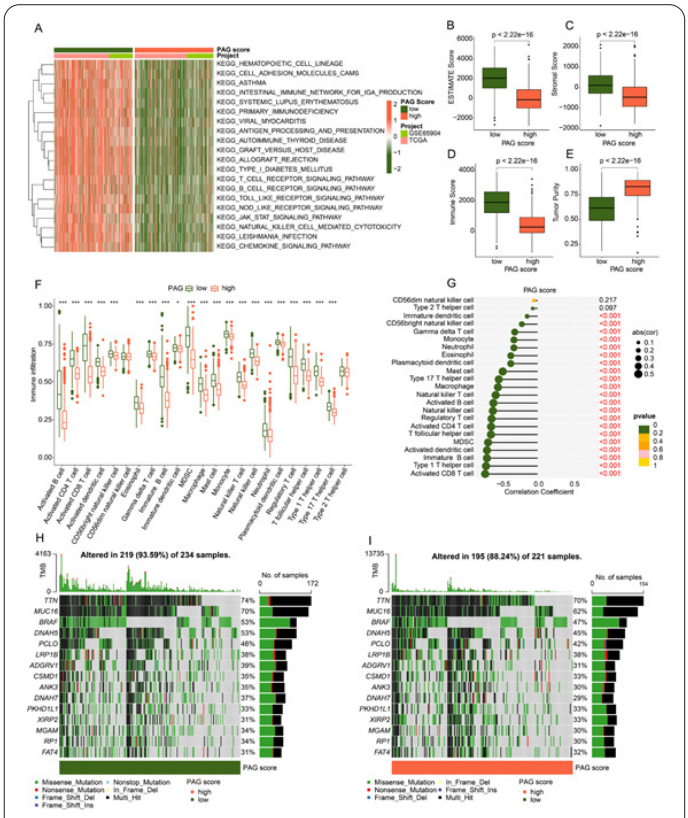

Figure 7. The relationship of PAG score and TME characteristic. (A) GSVA shows the KEGG pathways between low PAG score and high PSG score groups. (B-E) ESTIMATE, immune, stromal scores and tumor purity. (F) Immune infiltration assessment of 23 immune cells. (G) Correlation analysis of PAG score and TME characteristic. (H, I) Somatic mutation landscape in low- and high-PAG score groups.

groups was further investigated. The somatic mutation results revealed that the CM patients with low PAG scores had higher somatic mutation frequency, such as TTN (74%), MUC16 (70%), BRAF (53%), DNAH5 (53%), and PCLO (46%) (Figure 7H, I). These results demonstrated a markable difference in immune infiltration characteristics between the two PAG score groups, which may correlate with response to immunotherapy for CM.

Relationship between PAG score, immunotherapy and drug sensitivity

We further explored the relationship between PAG score and immunotherapy response. IPS analysis suggested the CM patients in the low PAG score group were more sensitive to the treatment of CTLA-4, PD-1 and CTLA-4/PD-1 (Figure 8A-D). Meanwhile, the immune response result showed that the TIDE score of CM with a high PAG score was significantly lower than those with a low PAG score, indicating a better response to immunotherapy for the high PAG score group (Figure 8E). The expression level of ICP indicated that most of the ICPs were markedly lower in the high PAG score group, which may explain the difference of immunotherapy for CM (Figure 8F). The correlation between PAG score and drug sensitivity was explored to select potential therapeutic drugs for CM. The results of IC50 distribution suggested that the high PAG score group had higher IC50 of rapamycin, paclitaxel, sunitinib, imatinib, cyclopamine, crizotinib, dasatinib, and doxorubicin, indicating a better drug sensitivity for CM patients with high PAG score (Figure 8G-N). Collectively, our results demonstrated a marked difference in immunotherapy and drug treatment of CM in different PAG score groups, giving a fresh insight for the future treatment of CM.

Discussion

In this study, we performed a molecular subtype analysis of CM based on PAGs. After screening for molecular differentially expressed PAGs, we established a PAGs signature that could effectively predict the prognosis of CM patients. The result suggested a possible role of PANoptosis in CM.

Although there is a lot of evidences showing the role of PANoptosis in the development of tumors, there is no clear study pointing to a drug mainly used by PANoptosis for the treatment of cancer (15). However, PANoptosis is involved in the therapeutic processes of many drugs. IFN-γ and TNF-α were reported to induce the death of various tumor cells including CM by PANoptosis (16). The role of many key factors of PANoptosis cannot be ignored either, such as ZBP1 and IRF1. In the mouse model, the combination of interferons and nuclear export inhibitors produced ZBP1-dependent PANoptosis that inhibited CM tumorigenesis (23). Hypermethylation of the ZBP1 promoter in breast cancer cells led to the downregulation of ZBP1 expression and increased proliferation and migration of cancer cells (24). These evidences suggest the antitumor activity of ZBP1. However, ZBP1 expression levels were also reported to be positively correlated with tumor aggressiveness (25). The heterogeneity among different tumors and the complexity of the functions of key factors of programmed cell death require careful selection of thera-

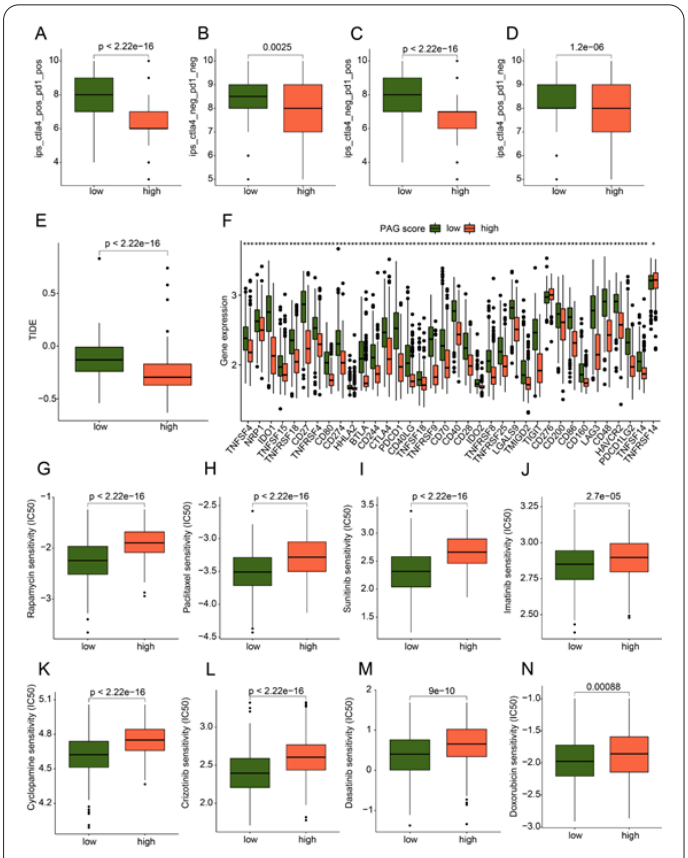

Figure 8. Analysis of immunotherapy response and drug sensitivity. (A-D) Relationship between PAG score and IPS score. (E) TIDE score. (F) Expression data of ICPs in low- and high PAG score groups. (G-N) Drug sensitivity analysis.

peutic targets. Furthermore, in gastric cancer, the PANoptosis pattern feature predicted gastric cancer survival and immunotherapy response (26). In CM, the key regulatory factor IRF1 of PANoptosis can be used as a biomarker to predict response to treatment with programmed cell death 1 (PD-1) axial ICI (27). In view of the great success of ICIs in CM treatment, the prediction of therapeutic effect of ICI by PANoptosis and even the induction of PANoptosis features in CM patients to cope with ICI treatment have potential theoretical basis.

Among the eight prognostic factors screened for the establishment of prognostic models, NAGK is an important member of the tumor-related metabolic reprogramming process. It influences tumor growth by participating in the phosphorylation of N-acetylglucosamine (28, 29). In addition, recent studies have shown that NAGK is essential for the activation of the host innate immune system by phosphorylating muramyl dipeptide so that it can be recognized (30). This suggests the role of NAGK in tumor immunity. The mentioned NAGK substrate, muramyl dipeptide, has been shown to act with other chemotherapy agents to inhibit tumor growth and metastasis, suggesting the possibility of NAGK as a therapeutic target (31, 32). The role of FBXO6 in tumors has also been incomprehensively reported. FBXO6 targets DNA damage checkpoint kinase CHK1 in order to destroy stagnant cells during the S phase and play a role in chemotherapy resistance (33). In ovarian cancer cells, depletion of FBXO6 promotes tumor proliferation, migration, and invasion (34). FBXO6 inhibits the progression of colorectal and gastric cancers by inducing RIOK1 ubiquitination (35). Our results suggest the tumor suppressive effect of FBXO6 in CM patients, which is in line with the effect in other cancer types.

Upregulation of CST7 expression is considered to be a marker of acute inflammation (36). The poor prognosis of CM patients with low CST7 expression levels may be related to low immune response levels. The role of PSME1 in modulating immune response has been extensively studied (37). In addition, the downregulation of PSME1 induced proteasome remodeling (38). Since proteasome expression is associated with better prognosis and response to checkpoint therapy in CM, further investigation of the association between lower PSME1 level and poorer prognosis in CM has positive clinical significance (39). USP3 plays a role in retarding tumor growth by reducing cdc25A protein levels through depletion and causing a significant delay in cell cycle progression (40). The role of RTN1 in tumors has not been reported.

The GO pathway enrichment analysis of PAGs showed that the lymphocyte-mediated immunity was the most significant difference in biological processes, suggesting the role of PAGs in tumor-related immune processes. The interaction between immune cells and tumors in TMEs plays a crucial role in tumor proliferation, immune escape and the development of drug resistance(41). We observed lower levels of infiltration of various immune components in TME in CM patients with poor prognosis. Not only B cells, $CD4^+$ T cells, $CD8^+$ T cells and other components promoting anti-tumor immunity, but also the proportion of components inducing immunosuppression such as regulatory T cells and MDSC also decreased(42). There is evidence that reduced disease progression and overall survival in melanoma patients can be attributed to the higher number and function of Tregs and MDSCs (43, 44). In addition to immune system failure in patients with high PAG scores, the observed reduction of various immune components may also be due to the suppression of multiple components of the immune system by screened PAG. The exact cause needs further evidence.

There are shortcomings in our research. The lack of *in vitro* and *in vivo* validation makes the results lack multicenter validation. In addition, the specific mechanism of the difference in prognosis has not been thoroughly studied. Further study on the role of selected targets in CM will deepen our understanding of the role of PANoptosis in tumorigenesis.

Funding

This work was supported by the Natural Science Foundation of Zhejiang Province (grant numbers LGF22H220006); the Projects of Medical and Health Technology Program in Zhejiang Province (grant numbers 2022KY119, 2021KY549 and 2022KY100).

Data availability

The datasets used in this study were obtained from the GTEx, TCGA and GEO databases. The original contributions presented in this study are included in the article. Further inquiries can be directed at the corresponding author.

Author Contributions

Like Zhong and Wenkang Qian conceived and designed the experiments; Like Zhong, Wangang Gong and Li Zhu carried out the studies and collected the data. Like Zhong performed the statistical analysis. Like Zhong and Xu Wang designed the study and wrote the manuscript. All authors have read and approved the final manuscript.

Conflicts of Interests

The authors declare no competing interests.

References

1. Whiteman DC, Green AC, Olsen CM. The Growing Burden of Invasive Melanoma: Projections of Incidence Rates and Numbers of New Cases in Six Susceptible Populations through 2031. J Invest Dermatol 2016; 136(6): 1161-1171.
2. Slominski RM, Sarna T, Plonka PM, Raman C, Brozyna AA, Slominski AT. Melanoma, Melanin, and Melanogenesis: The Yin and Yang Relationship. Front Oncol 2022; 12: 842496.
3. Slominski A, Kim TK, Brozyna AA, et al. The role of melanogenesis in regulation of melanoma behavior: melanogenesis leads to stimulation of HIF-1alpha expression and HIF-dependent attendant pathways. Arch Biochem Biophys 2014; 563: 79-93.
4. Siegel RL, Miller KD, Wagle NS, Jemal A. Cancer statistics, 2023. Ca-Cancer J Clin 2023; 73(1): 17-48.
5. Carlino MS, Larkin J, Long GV. Immune checkpoint inhibitors in melanoma. Lancet 2021; 398(10304): 1002-1014.
6. Brozyna AA, Jozwicki W, Roszkowski K, Filipiak J, Slominski AT. Melanin content in melanoma metastases affects the outcome of radiotherapy. Oncotarget 2016; 7(14): 17844-17853.
7. Slominski RM, Zmijewski MA, Slominski AT. The role of melanin pigment in melanoma. Exp Dermatol 2015; 24(4): 258-259.
8. Slominski RM, Raman C, Chen JY, Slominski AT. How cancer hijacks the body's homeostasis through the neuroendocrine system. Trends Neurosci 2023; 46(4): 263-275.
9. Slominski A, Zbytek B, Slominski R. Inhibitors of melanogenesis increase toxicity of cyclophosphamide and lymphocytes against

melanoma cells. Int J Cancer 2009; 124(6): 1470-1477.
10. Kuriakose T, Man SM, Malireddi RK, et al. ZBP1/DAI is an innate sensor of influenza virus triggering the NLRP3 inflammasome and programmed cell death pathways. Sci Immunol 2016; 1(2): aag2045.
11. Gurung P, Anand PK, Malireddi RK, et al. FADD and caspase-8 mediate priming and activation of the canonical and noncanonical Nlrp3 inflammasomes. J Immunol 2014; 192(4): 1835-1846.
12. Malireddi R, Gurung P, Kesavardhana S, et al. Innate immune priming in the absence of TAK1 drives RIPK1 kinase activity-independent pyroptosis, apoptosis, necroptosis, and inflammatory disease. J Exp Med 2020; 217(3): jem.20191644.
13. Wang Y, Kanneganti TD. From pyroptosis, apoptosis and necroptosis to PANoptosis: A mechanistic compendium of programmed cell death pathways. Comput Struct Biotec 2021; 19: 4641-4657.
14. Malireddi R, Kesavardhana S, Kanneganti TD. ZBP1 and TAK1: Master Regulators of NLRP3 Inflammasome/Pyroptosis, Apoptosis, and Necroptosis (PAN-optosis). Front Cell Infect Mi 2019; 9: 406.
15. Gong L, Huang D, Shi Y, Liang Z, Bu H. Regulated cell death in cancer: from pathogenesis to treatment. Chinese Med J-Peking 2023; 136(6): 653-665.
16. Malireddi R, Karki R, Sundaram B, et al. Inflammatory Cell Death, PANoptosis, Mediated by Cytokines in Diverse Cancer Lineages Inhibits Tumor Growth. Immunohorizons 2021; 5(7): 568-580.
17. Qi L, Wang L, Jin M, Jiang M, Li L, Li Y. Caspase-6 is a key regulator of cross-talk signal way in PANoptosis in cancer. Immunology 2023; 169(3): 245-259.
18. Zheng M, Karki R, Vogel P, Kanneganti TD. Caspase-6 Is a Key Regulator of Innate Immunity, Inflammasome Activation, and Host Defense. Cell 2020; 181(3): 674-687.
19. Schwarzer R, Laurien L, Pasparakis M. New insights into the regulation of apoptosis, necroptosis, and pyroptosis by receptor interacting protein kinase 1 and caspase-8. Curr Opin Cell Biol 2020; 63: 186-193.
20. Shao L, Hou W, Scharping NE, et al. IRF1 Inhibits Antitumor Immunity through the Upregulation of PD-L1 in the Tumor Cell. Cancer Immunol Res 2019; 7(8): 1258-1266.
21. Djulbegovic MB, Uversky VN. Expanding the understanding of the heterogeneous nature of melanoma with bioinformatics and disorder-based proteomics. Int J Biol Macromol 2020; 150: 1281-1293.
22. Ren H, Kang N, Yin S, Xu C, Qu T, Dai D. Characteristic of molecular subtypes based on PANoptosis-related genes and experimental verification of hepatocellular carcinoma. Aging (Albany Ny) 2023; 15(10): 4159-4181.
23. Karki R, Sundaram B, Sharma BR, et al. ADAR1 restricts ZBP1-mediated immune response and PANoptosis to promote tumorigenesis. Cell Rep 2021; 37(3): 109858.
24. Gu W, Pan F, Singer RH. Blocking beta-catenin binding to the ZBP1 promoter represses ZBP1 expression, leading to increased proliferation and migration of metastatic breast-cancer cells. J Cell Sci 2009; 122(Pt 11): 1895-1905.
25. Saez-Freire M, Blanco-Gomez A, Castillo-Lluva S, et al. The biological age linked to oxidative stress modifies breast cancer aggressiveness. Free Radical Bio Med 2018; 120: 133-146.
26. Pan H, Pan J, Li P, Gao J. Characterization of PANoptosis patterns predicts survival and immunotherapy response in gastric cancer. Clin Immunol 2022; 238: 109019.
27. Gupta S, McCann L, Chan Y, et al. Closed system RT-qPCR as a potential companion diagnostic test for immunotherapy outcome in metastatic melanoma. J Immunother Cancer 2019; 7(1): 254.
28. Chiaradonna F, Ricciardiello F, Palorini R. The Nutrient-Sensing Hexosamine Biosynthetic Pathway as the Hub of Cancer Metabolic Rewiring. Cells-Basel 2018; 7(6): 53.
29. Campbell S, Mesaros C, Izzo L, et al. Glutamine deprivation triggers NAGK-dependent hexosamine salvage. Elife 2021; 10: e62644.
30. Stafford CA, Gassauer AM, de Oliveira MC, et al. Phosphorylation of muramyl peptides by NAGK is required for NOD2 activation. Nature 2022; 609(7927): 590-596.
31. Harrison TS, Thompson NW. Multiple endocrine adenomatosis-I and II. Curr Prob Surg 1975: 1-51.
32. Wen X, Zheng P, Ma Y, et al. Salutaxel, a Conjugate of Docetaxel and a Muramyl Dipeptide (MDP) Analogue, Acts as Multifunctional Prodrug That Inhibits Tumor Growth and Metastasis. J Med Chem 2018; 61(4): 1519-1540.
33. Zhang YW, Brognard J, Coughlin C, et al. The F box protein Fbx6 regulates Chk1 stability and cellular sensitivity to replication stress. Mol Cell 2009; 35(4): 442-453.
34. Ji M, Zhao Z, Li Y, et al. FBXO6-mediated RNASET2 ubiquitination and degradation governs the development of ovarian cancer. Cell Death Dis 2021; 12(4): 317.
35. Hong X, Huang H, Qiu X, et al. Targeting posttranslational modifications of RIOK1 inhibits the progression of colorectal and gastric cancers. Elife 2018; 7: e29511.
36. Sawyer AJ, Garand M, Chaussabel D, Feng CG. Transcriptomic Profiling Identifies Neutrophil-Specific Upregulation of Cystatin F as a Marker of Acute Inflammation in Humans. Front Immunol 2021; 12: 634119.
37. Preckel T, Fung-Leung WP, Cai Z, et al. Impaired immunoproteasome assembly and immune responses in PA28-/- mice. Science 1999; 286(5447): 2162-2165.
38. Gu Y, Barwick BG, Shanmugam M, et al. Downregulation of PA28alpha induces proteasome remodeling and results in resistance to proteasome inhibitors in multiple myeloma. Blood Cancer J 2020; 10(12): 125.
39. Kalaora S, Lee JS, Barnea E, et al. Immunoproteasome expression is associated with better prognosis and response to checkpoint therapies in melanoma. Nat Commun 2020; 11(1): 896.
40. Das S, Chandrasekaran AP, Suresh B, et al. Genome-scale screening of deubiquitinase subfamily identifies USP3 as a stabilizer of Cdc25A regulating cell cycle in cancer. Cell Death Differ 2020; 27(11): 3004-3020.
41. Wu T, Dai Y. Tumor microenvironment and therapeutic response. Cancer Lett 2017; 387: 61-68.
42. Simiczyjew A, Dratkiewicz E, Mazurkiewicz J, Zietek M, Matkowski R, Nowak D. The Influence of Tumor Microenvironment on Immune Escape of Melanoma. Int J Mol Sci 2020; 21(21): 8359.
43. Ibrahim YS, Amin AH, Jawhar ZH, et al. "To be or not to Be": Regulatory T cells in melanoma. Int Immunopharmacol 2023; 118: 110093.
44. Jordan KR, Amaria RN, Ramirez O, et al. Myeloid-derived suppressor cells are associated with disease progression and decreased overall survival in advanced-stage melanoma patients. Cancer Immunol Immun 2013; 62(11): 1711-1722.